ESC European Society of Cardiology

European Heart Journal Open (2023) **3**, 1–12
https://doi.org/10.1093/ehjopen/oead090

ORIGINAL ARTICLE
Vascular and cardiac imaging

Novel near-infrared spectroscopy–intravascular ultrasound-based deep-learning methodology for accurate coronary computed tomography plaque quantification and characterization

Anantharaman Ramasamy[1,2], Hessam Sokooti[3], Xiaotong Zhang[4], Evangelia Tzorovili[5], Retesh Bajaj [1,2], Pieter Kitslaar[3,4], Alexander Broersen[4], Rajiv Amersey[1], Ajay Jain[1], Mick Ozkor[1], Johan H. C. Reiber [3,4], Jouke Dijkstra[4], Patrick W. Serruys[6,7], James C. Moon [1,8], Anthony Mathur [1,2], Andreas Baumbach [1,2], Ryo Torii [9], Francesca Pugliese [1,2], and Christos V. Bourantas [1,2,8,*]

[1]Department of Cardiology, Barts Heart Centre, Barts Health NHS Trust, West Smithfield, London EC1A 7BE, UK; [2]Centre for Cardiovascular Medicine and Devices, William Harvey Research Institute, Queen Mary University of London, Mile End Road, London E1 4NS, UK; [3]Medis Medical Imaging Systems, Leiden, The Netherlands; [4]Division of Image Processing, Department of Radiology, Leiden University Medical Center, Leiden, The Netherlands; [5]Pragmatic Clinical Trials Unit, Centre for Evaluation and Methods, Wolfson Institute of Population Health, Queen Mary University of London, London, UK; [6]Faculty of Medicine, National Heart and Lung Institute, Imperial College London, Cale Street, London SW3 6LY, UK; [7]Department of Cardiology, National University of Ireland, Galway, Ireland; [8]Institute of Cardiovascular Sciences, University College London, Gower Street, London WC1E 6BT, UK; and [9]Department of Mechanical Engineering, University College London, Torrington Place, London WC1E 7JE, UK

Received 12 June 2023; revised 16 July 2023; accepted 17 August 2023; online publish-ahead-of-print 30 October 2023

Aims Coronary computed tomography angiography (CCTA) is inferior to intravascular imaging in detecting plaque morphology and quantifying plaque burden. We aim to, for the first time, train a deep-learning (DL) methodology for accurate plaque quantification and characterization in CCTA using near-infrared spectroscopy–intravascular ultrasound (NIRS–IVUS).

Methods and results Seventy patients were prospectively recruited who underwent CCTA and NIRS–IVUS imaging. Corresponding cross sections were matched using an in-house developed software, and the estimations of NIRS–IVUS for the lumen, vessel wall borders, and plaque composition were used to train a convolutional neural network in 138 vessels. The performance was evaluated in 48 vessels and compared against the estimations of NIRS–IVUS and the conventional CCTA expert analysis. Sixty-four patients (186 vessels, 22 012 matched cross sections) were included. Deep-learning methodology provided estimations that were closer to NIRS–IVUS compared with the conventional approach for the total atheroma volume ($\Delta_{DL\text{-}NIRS\text{–}IVUS}$: -37.8 ± 89.0 vs. $\Delta_{Conv\text{-}NIRS\text{–}IVUS}$: 243.3 ± 183.7 mm3, variance ratio: 4.262, $P < 0.001$) and percentage atheroma volume (-3.34 ± 5.77 vs. 17.20 ± 7.20%, variance ratio: 1.578, $P < 0.001$). The DL methodology detected lesions more accurately than the conventional approach (Area under the curve (AUC): 0.77 vs. 0.67, $P < 0.001$) and quantified minimum lumen area ($\Delta_{DL\text{-}NIRS\text{–}IVUS}$: -0.35 ± 1.81 vs. $\Delta_{Conv\text{-}NIRS\text{–}IVUS}$: 1.37 ± 2.32 mm^2, variance ratio: 1.634, $P < 0.001$), maximum plaque burden (4.33 ± 11.83% vs. 5.77 ± 16.58%, variance ratio: 2.071, $P = 0.004$), and calcific burden (-51.2 ± 115.1 vs. -54.3 ± 144.4, variance ratio: 2.308, $P < 0.001$) more accurately than conventional approach. The DL methodology was able to segment a vessel on CCTA in 0.3 s.

Conclusions The DL methodology developed for CCTA analysis from co-registered NIRS–IVUS and CCTA data enables rapid and accurate assessment of lesion morphology and is superior to expert analysts (Clinicaltrials.gov: NCT03556644).

* Corresponding author. Tel: +44 20 7377 7000, Fax: +44 20 7791 9670, Emails: c.bourantas@nhs.net; c.bourantas@qmul.ac.uk

Graphical Abstract

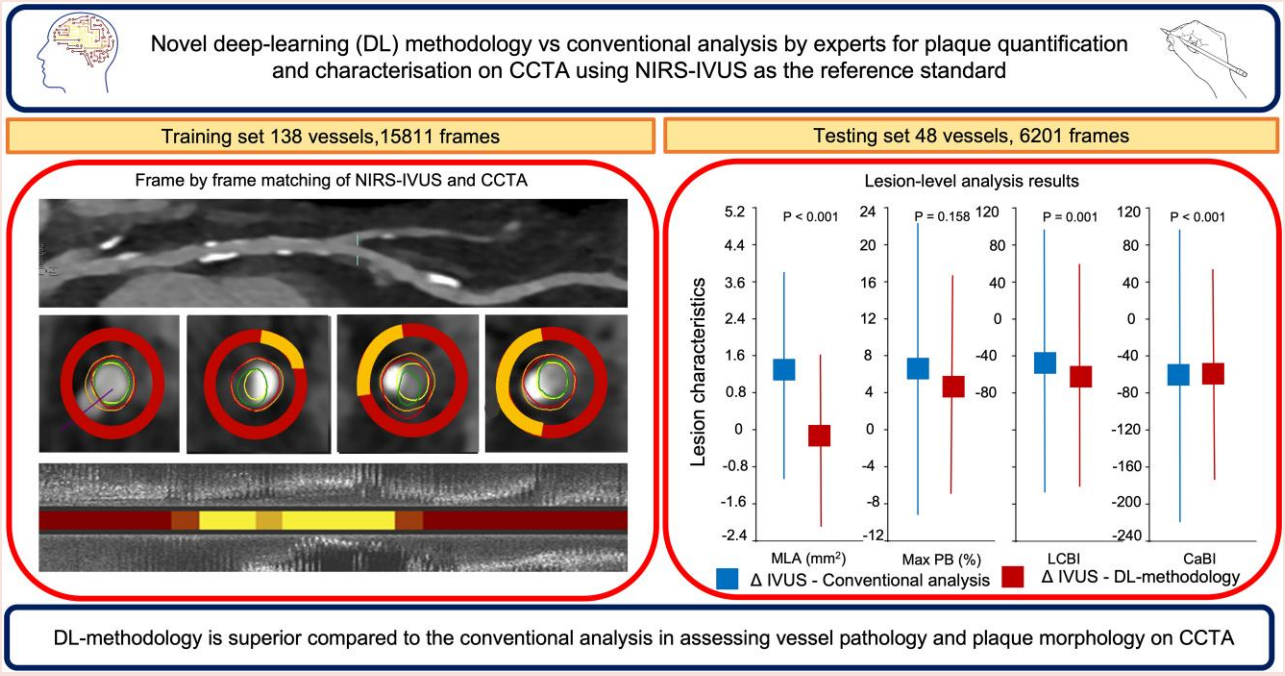

Keywords Coronary computed tomography angiography • Intravascular ultrasound • Deep learning • Near-infrared spectroscopy

Introduction

Coronary computed tomography angiography (CCTA) is an established non-invasive modality for quantifying and characterizing coronary atherosclerotic plaques with good diagnostic accuracy and high negative predictive value. Cumulative evidence has highlighted CCTA's potential to identify high-risk plaques—i.e. plaques that are prone to progress and cause cardiovascular events[1] and patients at risk,[2–5] however with limited efficacy, that is inferior to high-resolution intravascular imaging modalities.[6–8] Moreover, accurate CCTA analysis is time-consuming and labour-intensive which further limits its use in the study of atherosclerosis. To unlock the full potential of CCTA, accurate image analysis and acceleration of CCTA workflow are required.[9]

Deep-learning (DL) methodologies have revolutionized medical applications by facilitating rapid processing of large data sets. In the field of cardiac CT, the use of DL methods has enabled efficient data segmentation and reduced the time to diagnosis and analysis costs.[10–13] So far, DL methodologies in CCTA have been trained using expert annotations. However, CCTA has a limited accuracy in assessing atheroma characteristics and plaque burden (PB), while expert analysts are prone to errors and have weak reproducibility that can affect the performance of the developed DL methodologies.[14] Conversely, intravascular imaging modalities provide high-resolution images that enable more reproducible analysis and detailed assessment of atheroma characteristics and quantification of PB.[15–17] In this study, for the first time, we used the estimations of high-resolution near-infrared spectroscopy–intravascular ultrasound (NIRS–IVUS) to develop a novel DL methodology for accurate CCTA segmentation, plaque detection, and characterization.

Methods

Study population

In brief, 70 patients with chronic coronary syndrome and obstructive coronary artery disease (CAD) on invasive coronary angiography requiring further assessment or treatment with percutaneous coronary intervention (PCI) were prospectively recruited. All patients underwent CCTA prior to having three-vessel NIRS–IVUS imaging followed by a PCI as per clinical indication. The study has been specifically designed to optimize CCTA segmentation. The study was conducted in accordance with the Declaration of Helsinki, and the study protocol was approved by the local ethics committee (REC reference: 17/SC/0566). All participants provided written informed consent prior to study enrolment.

Coronary computed tomography angiography data acquisition

Coronary computed tomography angiography was performed using a 3rd-generation dual-source CT scanner (SOMATOM Force, Siemens Healthineers, Forchheim, Germany). Prior to CCTA imaging, participants received sub-lingual nitroglycerin (400 μg), and those with a heart rate > 70 b.p.m. were given intravenous metoprolol (maximum 40 mg), provided there were no contraindications. The scan parameters include prospective electrocardiogram-triggered sequential scan mode, gantry rotation time of 250 ms, 128 × 2 × 0.5 mm collimation with z-flying focal spot for both detectors, minimum tube voltage of 100 kV defined by the CarekV algorithm, and tube current determined by the scanner. Computed tomography calcium scoring images were not obtained to reduce radiation and in line with the objective of the study for plaque detection and characterization. The full CCTA scanning protocol has been described previously.[18] The

raw CCTA data were reconstructed with medium smooth kernel (b40f), slice thickness 0.50 mm with 0.30 mm increments, and highest strength model-based iterative reconstruction (ADMIRE 5) which allows the most accurate quantification of coronary atheroma.[19]

Near-infrared spectroscopy–intravascular ultrasound data acquisition

Near-infrared spectroscopy–intravascular ultrasound was performed in all three major epicardial vessels and where possible their side branches with a diameter ≥2 mm, using a 2.4F Makoto™ NIRS–IVUS 35–65 MHz Imaging System (Infraredx, Burlington, USA). The catheter was advanced to the distal vessel and pulled back at a constant speed of 0.5 mm/s with images acquired at 30 fps. Lesion pre-dilatation was performed prior to NIRS–IVUS imaging with a 2 mm semi-compliant balloon, only in cases of critical stenoses where the advancement of NIRS–IVUS probe was not possible, to facilitate NIRS–IVUS imaging. There were no complications from the NIRS–IVUS imaging during this study. The full NIRS–IVUS imaging protocol has been described previously.[18]

Near-infrared spectroscopy–intravascular ultrasound and coronary computed tomography angiography data analysis and co-registration

Coronary computed tomography angiography analysis was performed by an experienced analyst (cardiologist with an expertise in imaging)—with a known reproducibility—blinded to the IVUS analysis using a commercially available CT plaque analysis software (QAngio CT Research Edition 3.1, Medis Medical Imaging Systems, the Netherlands). The coronary tree was extracted, and the most proximal and distal side branches that were visible on both CCTA and NIRS–IVUS were used to define as a segment of interest. In each CCTA cross section within the segment of interest, the analyst manually annotated the lumen and vessel wall borders (conventional approach).

Stented segments were excluded from the analysis. In addition, segments with poor image quality, significant artefacts, and those that were pre-dilated (including the 5 mm proximal and distal segment) prior to NIRS–IVUS imaging were also excluded. Assessment of image quality was performed by two expert analysts; any disagreement was resolved by consensus.

Near-infrared spectroscopy–intravascular ultrasound segmentation was performed for the segment of interest by an independent analyst with an established reproducibility blinded to the CCTA data sets using the QCU-CMS software (version 4.69, Leiden University Medical Center, the Netherlands).[18] The IVUS end-diastolic frames were automatically extracted using an in-house DL methodology, and in these, the lumen and external elastic membrane (EEM) borders were manually detected.[18,20] Moreover, the presence and circumferential extent of the lipid core tissue in NIRS–IVUS frames was automatically extracted from the chemogram which is a two-dimensional (2D) colour-coded display of the lipid core distribution with the *x*-axis representing position along the length of the vessel and the *y*-axis position along its circumference. In addition, the circumferential distribution of the calcific tissue in each end-diastolic frame was manually annotated with an arc; calcific annotations were performed by two experienced analysts (A.R. and C.V.B.) whose reproducibility was tested in 220 frames. In these frames, the 1st analyst performed this analysis twice and the 2nd analyst once; these estimations were used to report the intra- and inter-observer variability. The agreement of the analysts for the presence of calcific tissue was assessed using the κ test of concordance, while the agreement of the analysts for the circumferential distribution of the calcific tissue was measured by estimating the mean ± standard deviation (SD) of the differences between the angles that defined its lateral extremities. Finally, the difference between the estimations of the analysts for the arc of calcium was used to assess their reproducibility for calcific tissue circumferential extent (expressed in degrees). Supplementary material online, *Table S1*, summarizes the findings of the reproducibility analysis; overall an excellent inter- and intra-observer agreement was found for the calcific tissue annotations.

The co-registration of CCTA and NIRS–IVUS cross sections was performed using an in-house, non-commercial software (QAngioCT IVUS Matcher, Medis Medical Imaging Systems Leiden, the Netherlands). This software enables simultaneous visualization of the CCTA and NIRS–IVUS images and matching of corresponding anatomical landmarks such as coronary ostia and side branches seen on both modalities. A linear interpolation was applied to co-register cross sections in between the matched landmarks. Every matched NIRS–IVUS cross section was then superimposed onto the corresponding CCTA frame to allow rotation and accurate alignment of the two modalities (*Figure 1*).

The correctly orientated lumen and EEM borders and the circumferential distribution of the lipid core and calcific tissue in NIRS–IVUS were treated as the reference standard and used to train DL methods for detecting the lumen and vessel wall borders and characterizing the composition of the plaque in CCTA.

Training of the deep-learning methodology

A data set of 138 vessels (49 patients) was used to train the DL methodology. The schematic design of the approach developed for the detection of the lumen and vessel wall in CCTA cross sections is given in *Figure 2*. The network architecture consists of a DenseUNet network with an input size of 64 × 64 × 7 voxels and an output size of 64 × 64 voxels and takes advantage of contextual information from three matched NIRS–IVUS frames before and after the centre frame to predict the lumen, the plaque, and the non-vessel (background) regions in the centre CTCA cross section. This is achieved using a softmax activation function, which forces each voxel to be classified in one of these three classes.

Several augmentations were applied during the optimization, such as flipping, rotation, moderate affine transformation, Gaussian noise, and Gamma transform. A post-processing stage was then implemented where the largest regions of each label were used to define the lumen and vessel wall borders.

The optimization was performed using Adam optimizer with a batch size of 256. The overt loss in the validation set was monitored, in which 15 patients are selected out of 49 patients (i.e. 30% of the training set). The best model weights were achieved after 142 epochs.

Plaque characterization in CCTA was performed using a convolutional neural network with a 2.5D U-Net architecture as proposed by Vu *et al.*[21]; in order to strengthen the connection between the different convolutional layers, the convolutional bloc were modified to dense blocks. In the final layers, 3D dense blocks were used to handle the concatenation of skip connections and were split into two branches to predict lipid cores and calcium tissue separately.

The cross-sectional CCTA images and the circumferential distribution of the lipid core and calcific tissue in the corresponding NIRS–IVUS frames were used as input for the network. For the lipid core estimations, the arcs that had a probability of ≥0.6 to indicate lipid cores in NIRS were treated as the ground truth. The lumen borders detected in CCTA images by the DL model developed for border detection were reduced by 1 mm and extended by 4 mm to define doughnut-shape regions of interest with a radius of 5 mm that were processed by the network to define plaque composition. A pixel-wise gradient sample weight was added to the loss function to make the network focus on the regions that were close to the lumen border (*Figure 2*). The final loss function is computed by the equation:

$$\text{loss} = \text{weight}_{\text{sample}} \times (\text{BCE}_{\text{lipid}} + \text{BCE}_{\text{calcium}} + \text{Aug}_{\text{kernel}}),$$

where $\text{weight}_{\text{sample}}$ denotes the pixel-wise gradient sample weight and $\text{BCE}_{\text{lipid}}$ and $\text{BCE}_{\text{calcium}}$ are binary cross entropy of lipid core and calcific tissue, respectively. To avoid over-fitting, a L2 norm regularization term $\text{Aug}_{\text{kernel}}$ with coefficient 1e-4 was added to each convolutional layer. Image augmentation such as flipping, rotation, and some small shifts was applied during the training.

The output of the developed DL method is the circumferential distribution of the lipid core tissue in one channel and of the calcific tissue in the second channel that are converted into one spread-out plot view similar to a NIRS chemogram with the *x*-axis indicating longitudinal position and the *y*-axis circumferential position of the detected tissue types.

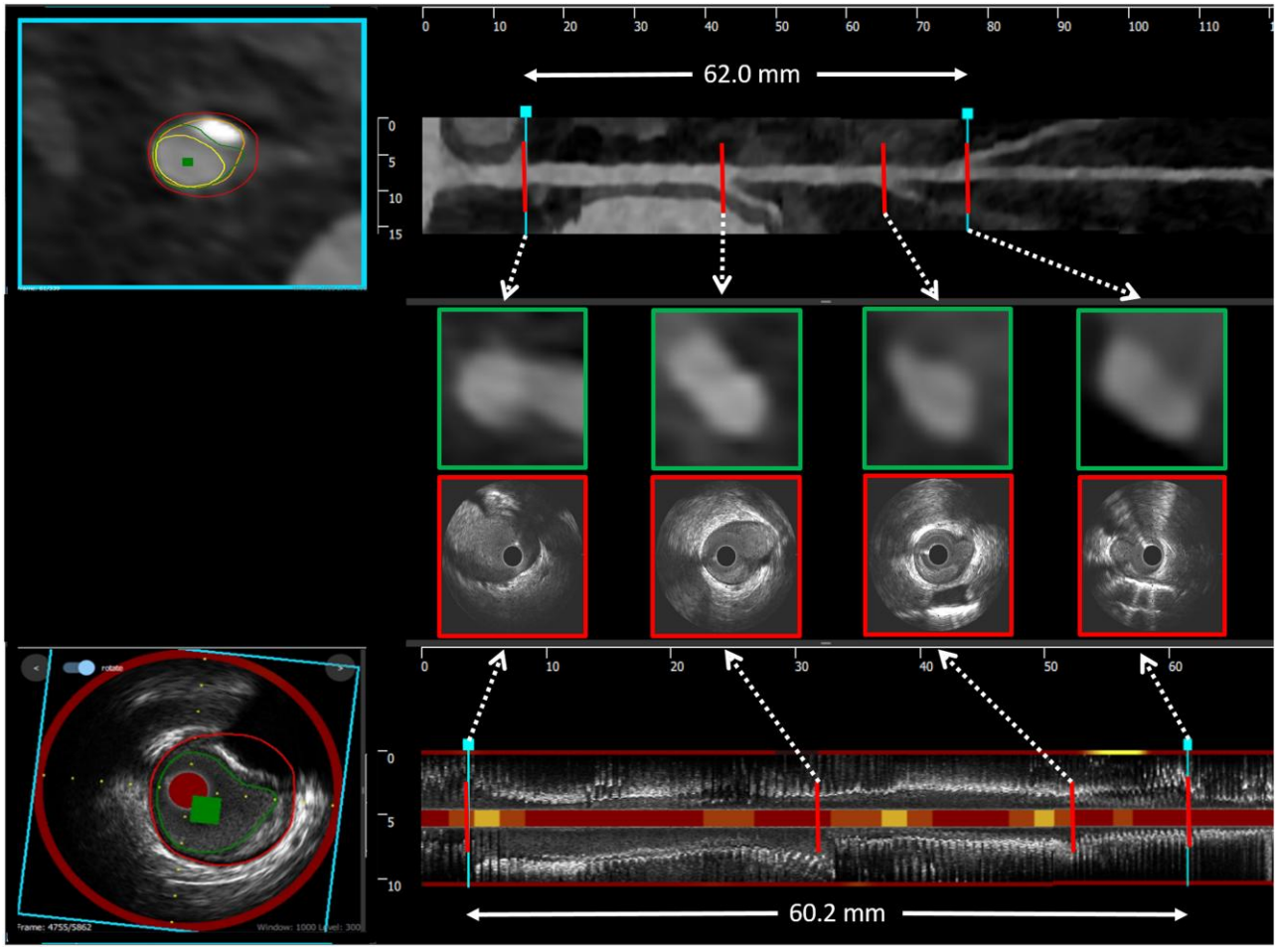

Figure 1 Intravascular ultrasound and coronary computed tomography angiography co-registration software. On the top panel, longitudinal view of a coronary computed tomography angiography segment of interest is shown with its corresponding longitudinal view on intravascular ultrasound on the bottom panel. Anatomical landmarks such as side branches are used to match the end-diastolic frames on intravascular ultrasound (red) and coronary computed tomography angiography cross sections (green) as shown the in the middle panel. The coronary computed tomography angiography frames in between the landmarks are interpolated. This software allows cross-sectional comparison between intravascular ultrasound and coronary computed tomography angiography. The left-hand side panel shows a corresponding coronary computed tomography angiography and intravascular ultrasound frames. The intravascular ultrasound frame is superimposed on the corresponding coronary computed tomography angiography cross section to allow rotation and accurate alignment between the two modalities; in this specific case, the intravascular ultrasound frame was titled 20° clockwise to match the corresponding coronary computed tomography angiography frame.

Comparison of the estimations of conventional analysis, deep-learning methodology, and near-infrared spectroscopy–intravascular ultrasound

The estimations of the conventional and the DL method were compared with the estimations of NIRS–IVUS in the test set of 48 vessels (15 patients) at segment level, lesion level, and cross-sectional levels:

- Segment-level analysis: For each segment of interest, the lumen, vessel, total atheroma volume (TAV) and per cent atheroma volume (PAV) were estimated by the conventional, the DL method, and the NIRS–IVUS and compared. The chemogram in NIRS–IVUS was used to estimate the lipid core burden index (LCBI) which corresponds to the fraction of pixels within the segment of interest that have ≥0.6 probability to portray lipid core tissue multiplied by 1000 and the maxLCBI$_{4mm}$ which is the maximum LCBI value within a 4-mm segment in the segment of interest.[22] The calcific burden index (CaBI) was estimated from the annotations of the calcific tissue in IVUS frames as the fraction of the calcific extent along the circumference and length of the segment of interest multiplied by 1000.[20] A similar approach was used in CCTA to compute in the conventional and DL method the LCBI, maxLCBI$_{4mm}$, and CaBI. On the conventional approach-established Hounsfield units (HU), cut-offs were used to define the presence of lipid (−30 to 75 HU) and calcific tissue (>350 HU) in CCTA images, and this information was plotted in 2D maps portraying in the *x*-axis the axial position of these tissues along the length of the artery and in the *y*-axis their circumferential position. Similar maps were constructed from the estimations of the DL method for the lipid and calcific tissue. The LCBI and CaBI were then calculated as the ratio of pixels of lipid and calcific tissue within the studied segment of interest multiplied by 1000.

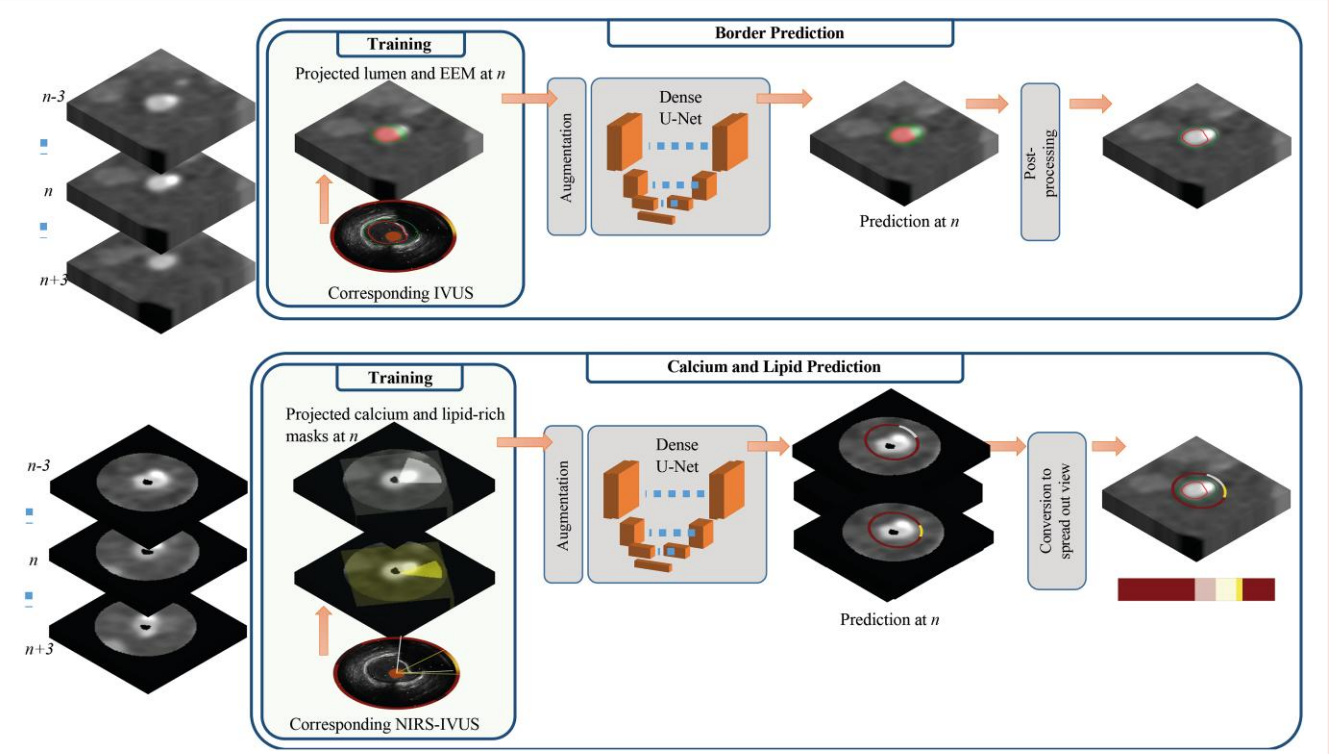

Figure 2 Schematic design of the deep-learning methodology developed for border detection and plaque characterization in coronary computed tomography angiography. The contextual information from three matched near-infrared spectroscopy–intravascular ultrasound frames before and after the centre frame (frame or cross section of interest) is used as input to predict the lumen area, plaque area, and background using a DenseUNet network. Post-processing of the detected areas is performed to define the lumen and vessel wall borders. In the second stage, the predicted lumen border is shrunk by 1 mm and extruded by 4 mm in these cross sections and defined area of interest together with the circumferential distribution of lipid core and calcific tissue in the corresponding near-infrared spectroscopy–intravascular ultrasound frames are utilized to train a DenseUNet network that estimates the circumferential distribution of the lipid and calcific tissue in the central coronary computed tomography angiography cross section. These estimations that are portrayed simultaneously in one spread-out plot, together with the lumen and vessel wall borders constitute the final output of the deep-learning methodology. EEM, external elastic membrane; IVUS, intravascular ultrasound; NIRS–IVUS, near-infrared spectroscopy–intravascular ultrasound.

- Lesion-level analysis: On NIRS–IVUS, a lesion was defined as a segment with a minimum PB ≥ 40% over three consecutive frames.[23,24] Lesions are identified as separate if there was a segment with a length > 5 mm between them. Receiver operating curve (ROC) analysis was performed in the output of the conventional and the DL method to identify the best cut-off that predicted a PB ≥ 40% on NIRS–IVUS, and this was used to define lesions in the test set. For each lesion, the following metrics were estimated and compared between NIRS–IVUS, the conventional, and the DL methods: lesion length, reference lumen, and vessel/EEM area (average of proximal and distal reference areas), minimum lumen area (MLA), vessel/EEM area at MLA, maximum PB, remodelling index, LCBI, $MaxLCBI_{4mm}$, and CaBI.
- Cross-sectional level analysis: the lumen, vessel/EEM, plaque area, and PB estimated in matched cross sections by NIRS–IVUS, the conventional, and DL methods were estimated and compared. In addition, morphological comparison between the estimations of the three approaches for the lumen and vessel/EEM borders was performed using the dice similarity coefficient (DSC), Hausdorff distance (HD), and mean distance.[16]

Statistical analysis

The distribution of continuous variables was assessed using the Kolmogorov–Smirnoff test. All continuous variables were normally distributed and presented as mean ± SD while categorical as absolute numbers and percentages. Continuous and categorical variables between the training and the test set were compared using independent sample *t*-test and χ^2 test, respectively. ROC curve analysis was used to examine the efficacy of the conventional and DL method for detecting a PB ≥ 40% on NIRS–IVUS and determining the best PB cut-off. This cut-off was used to define lesions in the output of the conventional and DL analysis.

Mixed-effect models with random intercepts by patient and by patient and vessel type were used to account for clustering effects between multiple lesions in the same vessel and multiple vessels in the same patient and were used to examine the effect of CCTA analysis (i.e. conventional method vs. DL method) on the agreement between NIRS–IVUS and CT estimations. For lesion-level analysis, vessel type was nested within patients. The mean differences, intra-class correlation coefficient (ICC), variance of differences, and Bland and Altman analyses were used to compare the estimations between the conventional and the DL methodology against NIRS–IVUS. Significance was assessed using the *F*-ratio test for the equality of variances. The confidence interval of the variance ratio was estimated using bootstrap re-sampling in 1500 samples. Mixed-effect models and variance ratio in the lesion-level analysis included all the available lesions even if measurements in the conventional or DL method were unavailable for some observations. Statistical analyses were performed using Stata version 17.0 (StataCorp LLC); the statistical significance was set at $P < 0.05$.

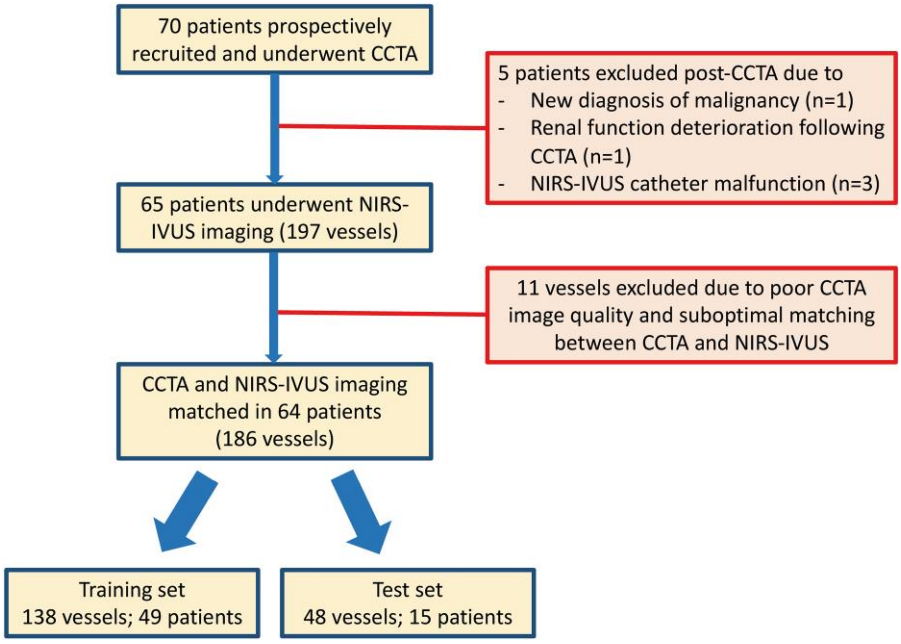

Figure 3 Study flowchart. CCTA, coronary computed tomography angiography; IVUS, intravascular ultrasound; NIRS–IVUS, near-infrared spectroscopy–intravascular ultrasound.

Table 1 Baseline demographics of the studied patients and vessels included in the analysis

	Studied vessels ($n = 64$)	Training set ($n = 49$)	Test set ($n = 15$)	*P*
Age (years)	62 ± 8	62 ± 9	61 ± 7	0.32
Gender (male)	5 (79.7%)	38 (77.6%)	13 (86.7%)	1.00
Current smoker	4 (6.3%)	3 (6.1%)	1 (6.7%)	1.00
Family history of CAD	40 (62.5%)	29 (59.2%)	11 (73.3%)	0.16
Co-morbidities				
Diabetes mellitus	22 (34.4%)	19 (38.8%)	3 (20.0%)	0.19
Hypertension	35 (54.7%)	30 (61.2%)	5 (33.3%)	0.11
Hypercholesterolaemia	45 (70.3%)	35 (71.4%)	10 (66.7%)	0.58
Renal failure[a]	14 (21.9%)	10 (20.4%)	4 (26.7%)	1.00
Previous PCI	14 (21.9%)	13 (26.5%)	1 (6.7%)	0.019
LV function				
Normal LV function	60 (93.8%)	46 (93.9%)	14 (93.3%)	0.33
Impaired LV function[b]	4 (6.3%)	3 (6.1%)	1 (6.7%)	0.33
Studied vessels				
Total number of frames	19 012	15 811	6201	
Total number of vessels	186	138	48	
LAD/diagonal branch	64 (34.4%)	48 (34.8%)	16 (33.3%)	
LCx/intermediate/obtuse marginal branch	78 (41.9%)	59 (42.8%)	19 (39.6%)	
RCA	44 (23.7%)	31 (22.5%)	13 (27.0%)	
Matched NIRS–IVUS and CCTA cross sections	22 012	15 811	6201	
LAD/diagonal branch	8284 (37.6%)	5922 (37.5%)	2362 (38.1%)	
LCx/intermediate/obtuse marginal branch	6510 (29.6%)	4896 (31.0%)	1614 (26.0%)	
RCA	7218 (32.8%)	4993 (31.6%)	2225 (35.9%)	

CAD, coronary artery disease; LAD, left anterior descending artery; LCx, left circumflex artery; LV, left ventricle; PCI, percutaneous coronary intervention; RCA, right coronary artery.
[a]Renal failure is defined as an estimated glomerular filtration rate of <60 mL/min/1.73 m2.
[b]Impaired LV function is defined as LV ejection fraction of 40–50%.

Table 2 Segment and lesion-level comparison of the estimations of intravascular ultrasound, conventional analysis, and deep-learning methodology

	NIRS–IVUS analysis	Conventional analysis	Δ NIRS–IVUS—conventional analysis	DL methodology	Δ IVUS—DL methodology	P[a]
Segment-level analysis						
Lumen volume (mm^3)	531.3 ± 462.9	398.8 ± 321.8	132.5 ± 148.5	492.8 ± 377.7	38.5 ± 112.0	0.19
Vessel volume (mm^3)	921.0 ± 707.6	545.2 ± 407.7	375.8 ± 310.6	920.3 ± 649.8	0.7 ± 126.3	0.001
TAV (mm^3)	389.7 ± 267.8	146.4 ± 109.4	243.3 ± 183.7	427.5 ± 279.9	−37.8 ± 89.0	<0.001
PAV (%)	44.20 ± 9.09	27.02 ± 10.95	17.20 ± 7.20	47.58 ± 5.55	−3.34 ± 5.77	<0.001
LCBI	50.0 ± 72.1	62.4 ± 72.9	−12.4 ± 84.2	73.1 ± 62.9	−23.1 ± 53.0	0.09
$MaxLCBI_{4mm}$	251.4 ± 201.2	265.9 ± 255.1	−14.5 ± 262.1	307.2 ± 204.8	−55.7 ± 213.9	0.28
CaBI	62.7 ± 62.2	56.7 ± 74.6	−5.97 ± 62.2	64.6 ± 81.8	−1.8 ± 37.3	0.60
Lesion-level analysis						
Lesion length (mm)	21.37 ± 18.60	14.16 ± 15.44	9.54 ± 15.63	17.29 ± 17.50	4.77 ± 18.43	0.01
Reference lumen area (mm^2)	10.71 ± 4.88	7.83 ± 3.49	3.97 ± 2.64	9.62 ± 3.87	1.93 ± 2.63	<0.001
Reference vessel/EEM area (mm^2)	15.11 ± 6.29	9.33 ± 4.03	7.36 ± 3.36	16.19 ± 6.32	−0.06 ± 3.55	<0.001
MLA (mm^2)	4.57 ± 3.43	3.29 ± 2.69	1.37 ± 2.32	4.55 ± 2.10	−0.35 ± 1.81	<0.001
Vessel/EEM at MLA (mm^2)	12.71 ± 6.14	8.25 ± 4.79	5.06 ± 4.82	11.97 ± 4.64	0.29 ± 3.08	<0.001
Maximum PB	64.82 ± 13.51	60.55 ± 19.03	5.77 ± 16.58	61.48 ± 9.72	4.33 ± 11.83	0.16
Remodelling index	0.84 ± 0.21	0.87 ± 0.29	−0.09 ± 0.30	0.82 ± 0.21	0.01 ± 0.20	0.58
LCBI	55.6 ± 79.8	103.2 ± 123.2	−46.2 ± 133.5	115.8 ± 106.9	−55.3 ± 122.8	0.001
$MaxLCBI_{4mm}$	189.2 ± 199.7	236.36 ± 237.2	−24.5 ± 258.3	282.1 ± 213.2	−62.3 ± 219.4	0.04
CaBI	97.7 ± 90.6	166.1 ± 158.2	−54.3 ± 144.4	154.5 ± 152.4	−51.2 ± 115.1	<0.001
Cross-sectional-level analysis						
Lumen area (mm^2)	8.54 ± 5.17	6.41 ± 3.77	2.12 ± 2.29	7.88 ± 4.05	0.66 ± 2.15	<0.001
EEM/vessel area (mm^2)	14.68 ± 7.33	8.74 ± 4.77	5.94 ± 3.72	14.71 ± 6.63	−0.03 ± 2.77	<0.001
Plaque area (mm^2)	6.15 ± 3.41	2.33 ± 2.36	3.81 ± 2.79	6.83 ± 3.12	−0.68 ± 2.21	<0.001
PB (%)	41.90 ± 14.90	25.41 ± 16.56	16.49 ± 14.87	46.74 ± 9.24	−4.83 ± 11.78	<0.001

CaBI, calcific burden index; DL, deep learning; EEM, external elastic membrane; IVUS, intravascular ultrasound; LCBI, lipid core burden index; MLA, minimum lumen area; PAV, percentage atheroma volume; PB, plaque burden; TAV, total atheroma volume.
[a]*P*-value derived from the mixed-effects model estimations.

Results

Sixty-four patients (197 vessels) had NIRS–IVUS and CCTA imaging and were included in the final analysis (*Figure 3*). Thirty-five patients (54.7%) suffered from hypertension, 45 patients (70.3%) suffered from hypercholesterolaemia, and 60 patients (93.8%) had preserved left ventricular systolic function. Patients in the training set were more likely to have had a previous PCI than the patients in the test set, but otherwise, there was no difference in baseline demographics of the two groups (*Table 1*).

From the 197 vessels assessed with CCTA, 11 were excluded due to motion artefacts (eight vessels) and extensive calcification (three vessels) which made CCTA analysis impossible. A total of 186 vessels (22 012 matched end-diastolic NIRS–IVUS frames and CCTA cross sections) were included in the analysis: 138 vessels (15 811 frames) were included in the training set, and 48 vessels (6201 frames) were included in the test set.

Segment-level analysis

Tables 2 and *3* summarize the findings of the segment-level analysis. The conventional approach underestimated lumen, vessel volume, TAV, and PAV, while the DL method provided closer estimations and had narrower limits of agreement with the estimations of NIRS–IVUS for these metrics (see Supplementary material online, *Figure S1*). Both the conventional method and especially the DL method overestimated the LCBI and $maxLCBI_{4mm}$ compared with NIRS–IVUS but provided similar estimations for the CaBI. Mixed-effect models showed that the type of CCTA segmentation (conventional method vs. DL method) had an effect on the agreement between CCTA and NIRS–IVUS for the vessel, TAV, and PAV suggesting a better performance of the DL method for these variables.

The ICC between NIRS–IVUS and DL method estimations was numerically higher than the ICC between NIRS–IVUS and the conventional approach for all the studied variables ($P < 0.001$ for all the variables, *Table 3*). Variance ratio of differences analysis indicated that the DL method had a higher agreement with NIRS–IVUS than the conventional approach for all the studied variables apart from the $maxLCBI_{4mm}$ and CaBI.

Lesion-level analysis

The best PB cut-off for detecting PB ≥ 40% in NIRS–IVUS was 27% in the conventional method and 49% in the DL method. Using these cut-offs, the conventional approach was able to detect 70.1% ($n = 61$) of the 87 lesions detected by NIRS–IVUS compared with the DL method, detecting 78.2% of the lesions ($n = 68$, $P < 0.001$, *Figure 4*). The DL method was also less likely to falsely detect lesions—identified seven

Table 3 Segment-, lesion-, and cross-sectional-level intra-class correlation coefficient and variance ratio of differences between the estimations of near-infrared spectroscopy–intravascular ultrasound, the conventional, and deep-learning methodology

	ICC between NIRS–IVUS and conventional analysis	*P*	ICC between NIRS–IVUS and DL methodology	*P*	Variance ratio of differences (95% CI)	P[a]
Segment-level analysis						
Lumen volume (mm^3)	0.938	<0.001	0.980	<0.001	1.757 (1.459–2.904)	<0.001
Vessel volume (mm^3)	0.829	<0.001	0.991	<0.001	4.262 (1.831–9.537)	<0.001
TAV (mm^3)	0.520	<0.001	0.969	<0.001	4.262 (1.831–9.534)	<0.001
PAV (%)	0.463	<0.001	0.786	<0.001	1.578 (1.032–2.449)	<0.001
LCBI	0.492	0.011	0.794	<0.001	2.517 (1.278–4.501)	0.002
$MaxLCBI_{4mm}$	0.522	0.007	0.605	0.001	1.500 (0.836–2.808)	0.17
CaBI	0.745	<0.001	0.931	<0.001	2.780 (0.652–8.172)	0.14
Lesion-level analysis						
Lesion length (mm)	0.683	<0.001	0.644	<0.001	0.719 (0.427–1.163)	0.20
Reference lumen area (mm^2)	0.721	<0.001	0.822	<0.001	1.006 (0.526– 1.838)	0.99
Reference vessel area (mm^2)	0.578	<0.001	0.897	<0.001	0.900 (0.399–2.048)	0.23
MLA (mm^2)	0.809	<0.001	0.828	<0.001	1.634 (1.147– 3.031)	0.001
Vessel/EEM area at MLA (mm^2)	0.625	<0.001	0.890	<0.001	2.447 (1.457–4.205)	0.001
Maximum PB (%)	0.691	<0.001	0.677	<0.001	2.071 (1.445–3.217)	0.004
Remodelling index	0.498	0.011	0.666	0.001	1.972 (0.823– 3.877)	0.14
LCBI	0.252	0.111	0.249	0.090	1.181 (0.603–2.233)	0.51
$MaxLCBI_{4mm}$	0.518	0.010	0.606	<0.001	1.418 (0.826–2.663)	0.23
CaBI	0.514	0.001	0.700	<0.001	2.308 (1.222–4.079)	0.002
Cross-sectional level analysis						
Lumen area (mm^2)	0.880	<0.001	0.939	<0.001	1.141 (1.104–1.180)	<0.001
Vessel volume (mm^2)	0.718	<0.001	0.959	<0.001	1.812 (1.742–1.885)	<0.001
Plaque area (mm^2)	0.456	<0.001	0.861	<0.001	1.601 (1.531–1.679)	<0.001
Plaque burden (%)	0.527	<0.001	0.676	<0.001	1.594 (1.535–1.652)	<0.001

CaBI, calcific burden index; DL, deep learning; EEM, external elastic membrane; ICC, intra-class correlation coefficient; IVUS, intravascular ultrasound; LCBI, lipid core burden index; MLA, minimum lumen area; PAV, percentage atheroma volume; PB, plaque burden; TAV, total atheroma volume.
[a]*P*-value derived from the variance ratio test.

lesions compared with the 14 lesions by the conventional approach that were not present on the NIRS–IVUS.

Mixed-effect model analysis demonstrated that the type of CCTA segmentation (i.e. conventional vs. DL) significantly influenced the agreement between CCTA and NIRS–IVUS for all the studied variables apart from the maximum PB and the remodelling index (*Table 2*). For lesion length, the bias was smaller, and the limits of agreement were narrower between conventional and NIRS–IVUS than DL and NIRS–IVUS estimations indicating that the conventional approach provides closer estimations to NIRS–IVUS than the DL method (see Supplementary material online, *Figure S2*). Conversely, the DL method appears to enable more accurate assessment of the reference lumen area, MLA, vessel wall area at the MLA, and CaBI than the conventional approach. Moreover, the DL method had a smaller bias and wider limits of agreement with NIRS–IVUS for the reference vessel area but a larger bias but narrower limits of agreement for the LCBI and $maxLCBI_{4mm}$ than the conventional approach.

The ICC between NIRS–IVUS and the conventional or the DL approach was statistically significant for all the lesion-based metrics (*Table 3*). The variance ratio of differences indicated that the DL method provides closer estimations to NIRS–IVUS than the conventional approach for the MLA, vessel area at the MLA, maximum PB, and CaBI.

Cross-sectional level analysis

The results of the cross-sectional level analysis are shown in *Tables 2* and *3* and Supplementary material online, *Figure S3*. The bias was smaller, and the limits of agreement between NIRS–IVUS and DL method were significantly narrower than the limits of agreement between NIRS–IVUS and the conventional approach, while the ICCs were higher for all the studied variables (*Table 3*). Mixed-effect model analysis and variance ratio of differences confirmed that the DL method is superior to the conventional approach for assessing the lumen, vessel wall, plaque area, and PB (see Supplementary material online, *Table S2*). Results were not different when analysis focused on frames with the presence of calcific and non-calcific tissues (see Supplementary material online, *Table S3*).

Manual CCTA segmentation (accurate annotation of every lumen and vessel wall border) of a 70-mm segment takes ~5 h, while the DL methodology is able to estimate the lumen and vessel wall borders and characterize plaque composition within 40 s.

Discussion

In this study, for the first time, we introduced a DL methodology trained from co-registered NIRS–IVUS and CCTA data to detect the

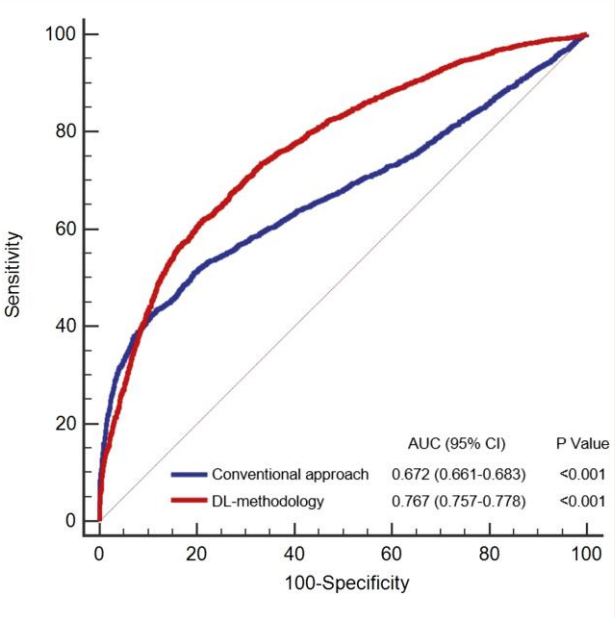

Figure 4 Receiver operating curve analysis showing the efficacy of the conventional approach and deep-learning methodology for detecting lesions using near-infrared spectroscopy–intravascular ultrasound as the gold standard. AUC: Area under the curve.

lumen and vessel wall borders and quantify PB and composition in CCTA. We found that the developed method (i) enables more accurate volumetric analyses of the segment of interest in CCTA than the conventional analysis, (ii) has higher accuracy in detecting lesions and assessing the MLA and maximum PB, (iii) more accurately measures calcific burden and narrow limits of agreement but larger bias for the estimations of lipid burden than the conventional approach that relies on established HU cut-offs, and (iv) is fast, allowing fully automated and reproducible segmentation and plaque characterization of the coronary tree in a few seconds (see Supplementary material online, *Videos S1* and *S2*).

Several methodologies have been introduced for automated segmentation of CCTA data.[11–13,25,26] However, these approaches have limitations as some focused on assessing lesion severity,[12] and some are only capable to provide qualitative information about plaque phenotypes without measuring the PB,[11,25] and others estimate vessel wall dimensions but cannot accurately characterize plaque morphology.[13] More importantly, all these methods have been trained and tested against expert analysts, who have limited reproducibility and limited efficacy in quantifying PB and phenotype[27,28] while the only method that used intravascular imaging to train a DL method for differentiating lipid-rich from non-lipid-rich plaques in CCTA utilized integrated backscatter IVUS analysis—a modality that is not widely available—and failed to demonstrate a superiority of the DL method over the human experts in assessing plaque composition.[29]

Our prospective study introduces a paradigm shift in coronary image analysis. We propose the use of intravascular imaging and, in particular, of NIRS–IVUS—the only FDA-approved modality for detecting high-risk lesions to train a DL methodology for more accurate analysis of CCTA. In contrast to previous studies comparing intravascular imaging and CCTA,[27,28] NIRS–IVUS was performed in all the major epicardial arteries, irrespective of the presence of disease providing an ideal set for training of a DL method. Moreover, we took advantage of a well-validated DL approach to identify the end-diastolic frames in NIRS–IVUS and match these with the CCTA cross sections. The use of end-diastolic NIRS–IVUS frames minimized errors in data co-registration introduced by the longitudinal motion of the IVUS catheter[30] and enabled more reproducible assessment of the lumen dimensions, as these changes up to 10% during the cardiac cycle.[31–33] Finally, we designed a special module to co-register NIRS–IVUS and CCTA data that allow superimposition and rotational alignment of the lumen and EEM borders and of the estimations of NIRS–IVUS for the lipid core and calcific tissue on CCTA. These advances enable accurate data co-registration that was used to train DL algorithms for image segmentation and plaque characterization in CCTA.

Testing at a segment level demonstrated that the DL method is superior to conventional CCTA analysis for quantifying vessel wall volume and, more importantly, TAV and PAV which are commonly used in serial coronary imaging studies to assess the efficacy of novel therapies targeting atherosclerosis.[34–37] In addition, we included all vessels, including normal or with minor coronary artery disease irrespective of their disease burden, which reflects the vast majority of patients undergoing CCTA in clinical practice. The DL method appears capable to assess LCBI which is an established predictor of worse outcomes in recent studies[38] but is not superior to the conventional approach for the maxLCBI$_{4mm}$ and CaBI. These advantages and the fact that the DL method is fast have been incorporated in a user-friendly commercially available software (QAngioCT Research Edition) and provide a fully reproducible analysis, which renders it as the ideal methodology for risk stratification and segmentation of serial data collected in studies assessing the efficacy of novel pharmacotherapies.

Results were similar when analysis was performed at a lesion level. The DL methodology was superior to the conventional approach in detecting lesions and allowed a more accurate assessment of the MLA and maximum PB which are established predictors of plaque vulnerability. Moreover, the DL method enabled more accurate quantification of the CaBI that is important in treatment planning. Conversely, both approaches had limited efficacy in measuring lesion length and the references lumen and vessel area as well as the lipid component (i.e. LCBI and maxLCBI$_{4mm}$). The large discrepancy between CCTA and NIRS–IVUS estimations for lesion length and the reference lumen and vessel areas should at least partially be attributed to the present of tandem lesions on NIRS–IVUS, which occasionally in CCTA analysis appear as one long lesion; conversely, many long lesions in NIRS–IVUS were often classified as tandem lesion in CCTA. Moreover, the limited efficacy of the conventional and the DL methods in detecting lipid core plaques is due to the fact that image features have limited value in assessing the biochemical composition of lipid tissue as NIRS imaging. This is a well-known limitation, not only of CCTA but also of intravascular imaging,[17] and was even more apparent in mixed plaques where the blooming artefacts from the calcium mask the surrounding tissues (*Figure 5*).

Limitations

Firstly, the number of vessels that were included for the training and testing of the DL algorithms are relatively small; a larger training set is expected to enhance the performance of the developed method and improve the segmentation and plaque characterization in CCTA. Secondly, despite the fact that an effort was made to optimize NIRS–IVUS and CCTA image co-registration by selecting only end-diastolic NIRS–IVUS frames, it is likely the lumen and vessel morphologies to have been distorted in some NIRS–IVUS frames by the intravascular imaging catheter; this is more likely to have occurred in tortuous and angulated vessels resulting in erroneous estimations of the lumen and vessel wall borders. Thirdly, although the proposed DL method was superior to the conventional approach for detecting lipid cores, its

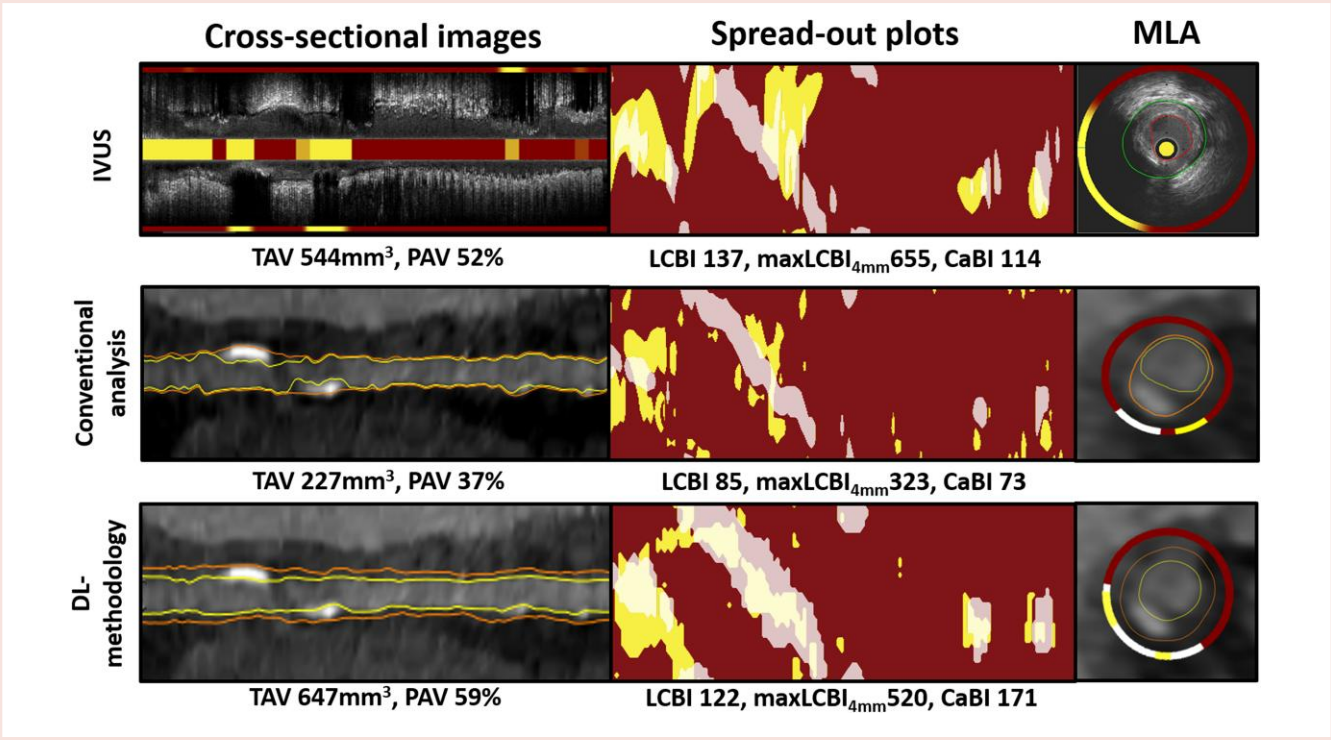

Figure 5 Lumen, vessel wall, and plaque component estimations of the conventional and deep-learning method. The top panel portrays a longitudinal cross section of the segment of interest in a left circumflex coronary artery on near-infrared spectroscopy–intravascular ultrasound, the middle panel portrays the corresponding segment in coronary computed tomography angiography with the lumen and vessel wall borders detected by the conventional approach, and the bottom panel shows the output of the deep-learning method. The per cent atheroma volume and total atheroma volume estimations are also shown. The corresponding distribution of plaque components for the near-infrared spectroscopy–intravascular ultrasound, the conventional approach, and the deep-learning method are portrayed as spread-out plots (yellow indicating presence of lipid core and semi-transparent white showing the presence of calcific tissue) along with the estimations of lipid core burden index, max$LCBI_{4mm}$ and calcific burden index. Lastly, the corresponding cross section portraying the minimum lumen area with lumen, vessel wall borders, and plaque components detected by each approaches is shown. CaBI, calcific burden index; DL, deep learning; LCBI, lipid core burden index; PAV, per cent atheroma volume; TAV, total atheroma volume.

correlation with NIRS–IVUS estimations remains weak. Moreover, the methodology developed for plaque characterization in CCTA is unable to provide information about the thickness and depth of the lipid cores in the plaque as it relies on NIRS–IVUS which only gives information about its circumferential extent. Additionally, the developed DL method was trained and tested on data collected by a 3rd-generation CCTA scanner with a specific reconstruction approach. It is unclear whether the findings of this analysis can be generalized to CCTA images collected by different vendors. Finally, although superior to conventional CCTA segmentation, it's unclear whether the DL methodology allows more accurate detection of high-risk lesions and patients, which requires a large-scale study.

Conclusions

We developed a novel DL methodology that was trained from the estimations of NIRS–IVUS to accurately estimate the lumen and vessel wall dimensions and quantify PB and composition in CCTA images. The proposed methodology appears superior to the conventional analysis performed by experts in assessing vessel pathology and morphology and may have the potential to enhance the applications of CCTA in guiding PCI, assessing the efficacy of novel pharmacotherapies in inhibiting plaque progression, and stratifying cardiovascular risk.

Lead author biography

Professor Christos Bourantas graduated from the medical school, University of Ioannina, and received his PhD degree from the same university in 2005. He completed his cardiology training in 2011 in the UK, followed by a post-doc research fellowship in Thorax Centre, Erasmus Medical Centre, and a post-CCT fellowship in interventional cardiology in Newcastle. He is a consultant interventional cardiologist at Barts Health NHS Trust, UK. He has a strong interest in research, education, and training and he is currently an honorary Professor at Queen Mary University of London. His research interests focus on invasive and non-invasive cardiovascular imaging, computational modelling, vulnerable plaque detection, and secondary prevention.

Data availability

The data will be shared on reasonable request to the corresponding author.

Supplementary material

Supplementary material is available at *European Heart Journal Open* online.

Funding

This study is jointly funded by British Heart Foundation (PG/17/18/32883), University College London Biomedical Resource Centre (BRC492B), and Rosetrees Trust (A1773). A.R., R.B., A.M., A.B., and C.V.B. are funded by Barts NIHR Biomedical Research Centre, London, UK.

Conflict of interest: None declared.

References

1. Naghavi M, Libby P, Falk E, Casscells SW, Litovsky S, Rumberger J, Badimon JJ, Stefanadis C, Moreno P, Pasterkamp G, Fayad Z, Stone PH, Waxman S, Raggi P, Madjid M, Zarrabi A, Burke A, Yuan C, Fitzgerald PJ, Siscovick DS, de Korte CL, Aikawa M, Juhani Airaksinen KE, Assmann G, Becker CR, Chesebro JH, Farb A, Galis ZS, Jackson C, Jang IK, Koenig W, Lodder RA, March K, Demirovic J, Navab M, Priori SG, Rekhter MD, Bahr R, Grundy SM, Mehran R, Colombo A, Boerwinkle E, Ballantyne C, Insull W Jr, Schwartz RS, Vogel R, Serruys PW, Hansson GK, Faxon DP, Kaul S, Drexler H, Greenland P, Muller JE, Virmani R, Ridker PM, Zipes DP, Shah PK, Willerson JT. From vulnerable plaque to vulnerable patient: a call for new definitions and risk assessment strategies: part I. *Circulation* 2003;**108**:1664–1672.
2. Ferencik M, Mayrhofer T, Bittner DO, Emami H, Puchner SB, Lu MT, Meyersohn NM, Ivanov AV, Adami EC, Patel MR, Mark DB, Udelson JE, Lee KL, Douglas PS, Hoffmann U. Use of high-risk coronary atherosclerotic plaque detection for risk stratification of patients with stable chest pain: a secondary analysis of the PROMISE randomized clinical trial. *JAMA Cardiol* 2018;**3**:144–152.
3. Motoyama S, Sarai M, Harigaya H, Anno H, Inoue K, Hara T, Naruse H, Ishii J, Hishida H, Wong ND, Virmani R, Kondo T, Ozaki Y, Narula J. Computed tomographic angiography characteristics of atherosclerotic plaques subsequently resulting in acute coronary syndrome. *J Am Coll Cardiol* 2009;**54**:49–57.
4. Newby DE, Adamson PD, Berry C, Boon NA, Dweck MR, Flather M, Forbes J, Hunter A, Lewis S, MacLean S, Mills NL, Norrie J, Roditi G, Shah ASV, Timmis AD, van Beek EJR, Williams MC. Coronary CT angiography and 5-year risk of myocardial infarction. *N Engl J Med* 2018;**379**:924–933.
5. SCOT-HEART investigators. CT coronary angiography in patients with suspected angina due to coronary heart disease (SCOT-HEART): an open-label, parallel-group, multicentre trial. *Lancet*. 2015;**385**:2383–2391.
6. Prati F, Romagnoli E, Gatto L, La Manna A, Burzotta F, Ozaki Y, Marco V, Boi A, Fineschi M, Fabbiocchi F, Taglieri N, Niccoli G, Trani C, Versaci F, Calligaris G, Ruscica G, Di Giorgio A, Vergallo R, Albertucci M, Biondi-Zoccai G, Tamburino C, Crea F, Alfonso F, Arbustini E. Relationship between coronary plaque morphology of the left anterior descending artery and 12 months clinical outcome: the CLIMA study. *Eur Heart J* 2020;**41**:383–391.
7. Erlinge D, Maehara A, Ben-Yehuda O, Bøtker HE, Maeng M, Kjøller-Hansen L, Engstrøm T, Matsumura M, Crowley A, Dressler O, Mintz GS, Fröbert O, Persson J, Wiseth R, Larsen AI, Okkels Jensen L, Nordrehaug JE, Bleie Ø, Omerovic E, Held C, James SK, Ali ZA, Muller JE, Stone GW. Identification of vulnerable plaques and patients by intracoronary near-infrared spectroscopy and ultrasound (PROSPECT II): a prospective natural history study. *Lancet* 2021;**397**:985–995.
8. Waksman R, Di Mario C, Torguson R, Ali ZA, Singh V, Skinner WH, Artis AK, Cate TT, Powers E, Kim C, Regar E, Wong SC, Lewis S, Wykrzykowska J, Dube S, Kazziha S, van der Ent M, Shah P, Craig PE, Zou Q, Kolm P, Brewer HB, Garcia-Garcia HM, Investigators LRP. Identification of patients and plaques vulnerable to future coronary events with near-infrared spectroscopy intravascular ultrasound imaging: a prospective, cohort study. *Lancet* 2019;**394**:1629–1637.
9. Knuuti J, Wijns W, Saraste A, Capodanno D, Barbato E, Funck-Brentano C, Prescott E, Storey RF, Deaton C, Cuisset T, Agewall S, Dickstein K, Edvardsen T, Escaned J, Gersh BJ, Svitil P, Gilard M, Hasdai D, Hatala R, Mahfoud F, Masip J, Muneretto C, Valgimigli M, Achenbach S, Bax JJ. 2019 ESC guidelines for the diagnosis and management of chronic coronary syndromes. *Eur Heart J* 2020;**41**:407–477.
10. Muscogiuri G, Chiesa M, Trotta M, Gatti M, Palmisano V, Dell'Aversana S, Baessato F, Cavaliere A, Cicala G, Loffreno A, Rizzon G, Guglielmo M, Baggiano A, Fusini L, Saba L, Andreini D, Pepi M, Rabbat MG, Guaricci AI, De Cecco CN, Colombo G, Pontone G. Performance of a deep learning algorithm for the evaluation of CAD-RADS classification with CCTA. *Atherosclerosis* 2020;**294**:25–32.
11. Zreik M, van Hamersvelt RW, Wolterink JM, Leiner T, Viergever MA, Isgum I. A recurrent CNN for automatic detection and classification of coronary artery plaque and stenosis in coronary CT angiography. *IEEE Trans Med Imaging* 2019;**38**:1588–1598.
12. Kang D, Dey D, Slomka PJ, Arsanjani R, Nakazato R, Ko H, Berman DS, Li D, Kuo CC. Structured learning algorithm for detection of nonobstructive and obstructive coronary plaque lesions from computed tomography angiography. *J Med Imaging (Bellingham)* 2015;**2**:014003.
13. Lin A, Manral N, McElhinney P, Killekar A, Matsumoto H, Kwiecinski J, Pieszko K, Razipour A, Grodecki K, Park C, Otaki Y, Doris M, Kwan AC, Han D, Kuronuma K, Flores Tomasino G, Tzolos E, Shanbhag A, Goeller M, Marwan M, Gransar H, Tamarappoo BK, Cadet S, Achenbach S, Nicholls SJ, Wong DT, Berman DS, Dweck M, Newby DE, Williams MC, Slomka PJ, Dey D. Deep learning-enabled coronary CT angiography for plaque and stenosis quantification and cardiac risk prediction: an international multicentre study. *Lancet Digit Health* 2022;**4**:e256–e265.
14. Kim C, Hong SJ, Shin DH, Kim JS, Kim BK, Ko YG, Choi D, Jang Y, Hong MK. Limitations of coronary computed tomographic angiography for delineating the lumen and vessel contours of coronary arteries in patients with stable angina. *Eur Heart J Cardiovasc Imaging* 2015;**16**:1358–1365.
15. Rodriguez-Granillo GA, Vaina S, García-García HM, Valgimigli M, Duckers E, van Geuns RJ, Regar E, van der Giessen WJ, Bressers M, Goedhart D, Morel MA, de Feyter PJ, Serruys PW. Reproducibility of intravascular ultrasound radiofrequency data analysis: implications for the design of longitudinal studies. *Int J Cardiovasc Imaging* 2006;**22**:621–631.
16. Bajaj R, Huang X, Kilic Y, Ramasamy A, Jain A, Ozkor M, Tufaro V, Safi H, Erdogan E, Serruys PW, Moon J, Pugliese F, Mathur A, Torii R, Baumbach A, Dijkstra J, Zhang Q, Bourantas CV. Advanced deep learning methodology for accurate, real-time segmentation of high-resolution intravascular ultrasound images. *Int J Cardiol* 2021;**339**:185–191.
17. Ramasamy A, Serruys PW, Jones DA, Johnson TW, Torii R, Madden SP, Amersey R, Krams R, Baumbach A, Mathur A, Bourantas CV. Reliable in vivo intravascular imaging plaque characterization: a challenge unmet. *Am Heart J* 2019;**218**:20–31.
18. Ramasamy A, Safi H, Moon JC, Andiapen M, Rathod KS, Maurovich-Horvat P, Bajaj R, Serruys PW, Mathur A, Baumbach A, Pugliese F, Torii R, Bourantas CV. Evaluation of the efficacy of computed tomographic coronary angiography in assessing coronary artery morphology and physiology: rationale and study design. *Cardiology* 2020;**145**:285–293.
19. Ramasamy A, Hamid AKA, Cooper J, Simon J, Maurovich-Horvat P, Bajaj R, Kitslaar P, Amersey R, Jain A, Deaner A, Reiber JH, Moon JC, Dijkstra J, Serruys PW, Mathur A, Baumbach A, Torii R, Pugliese F, Bourantas CV. Implications of computed tomography reconstruction algorithms on coronary atheroma quantification: comparison with intravascular ultrasound. *J Cardiovasc Comput Tomogr* 2022;**17**:43–51.
20. Bourantas CV, Serruys PW, Nakatani S, Zhang YJ, Farooq V, Diletti R, Ligthart J, Sheehy A, van Geuns RJ, McClean D, Chevalier B, Windecker S, Koolen J, Ormiston J, Whitbourn R, Rapoza R, Veldhof S, Onuma Y, Garcia-Garcia HM. Bioresorbable vascular scaffold treatment induces the formation of neointimal cap that seals the underlying plaque without compromising the luminal dimensions: a concept based on serial optical coherence tomography data. *EuroIntervention* 2015;**11**:746–756.
21. Vu MH, Grimbergen G, Nyholm T, Löfstedt T. Evaluation of multislice inputs to convolutional neural networks for medical image segmentation. *Med Phys* 2020;**47**:6216–6231.
22. Goldstein JA, Madden SP, Sum ST, Dixon SR, Madder RD, Muller JE. Assessment of plaque composition with near-infrared spectroscopy. *Curr Cardiovasc Imaging Rep* 2011;**4**:298–308.
23. Stone GW, Maehara A, Lansky AJ, de Bruyne B, Cristea E, Mintz GS, Mehran R, McPherson J, Farhat N, Marso SP, Parise H, Templin B, White R, Zhang Z, Serruys PW. A prospective natural-history study of coronary atherosclerosis. *N Engl J Med* 2011;**364**:226–235.
24. Garcia-Garcia HM, Gomez-Lara J, Gonzalo N, Garg S, Shin ES, Goedhart D, Serruys PW. A comparison of the distribution of necrotic core in bifurcation and non-bifurcation coronary lesions: an in vivo assessment using intravascular ultrasound radiofrequency data analysis. *EuroIntervention* 2010;**6**:321–327.
25. Choi AD, Marques H, Kumar V, Griffin WF, Rahban H, Karlsberg RP, Zeman RK, Katz RJ, Earls JP. CT evaluation by artificial intelligence for atherosclerosis, stenosis and vascular morphology (CLARIFY): a multi-center, international study. *J Cardiovasc Comput Tomogr* 2021;**15**:470–476.
26. Hong Y, Commandeur F, Cadet S, Goeller M, Doris MK, Chen X, Kwiecinski J, Berman DS, Slomka PJ, Chang HJ, Dey D. Deep learning-based stenosis quantification from coronary CT angiography. *Proc SPIE Int Soc Opt Eng* 2019;**10949**:109492I.
27. Voros S, Rinehart S, Qian Z, Joshi P, Vazquez G, Fischer C, Belur P, Hulten E, Villines TC. Coronary atherosclerosis imaging by coronary CT angiography: current status, correlation with intravascular interrogation and meta-analysis. *JACC Cardiovasc Imaging* 2011;**4**:537–548.
28. Fischer C, Hulten E, Belur P, Smith R, Voros S, Villines TC. Coronary CT angiography versus intravascular ultrasound for estimation of coronary stenosis and atherosclerotic plaque burden: a meta-analysis. *J Cardiovasc Comput Tomogr* 2013;**7**:256–266.
29. Masuda T, Nakaura T, Funama Y, Oda S, Okimoto T, Sato T, Noda N, Yoshiura T, Baba Y, Arao S, Hiratsuka J, Awai K. Deep learning with convolutional neural network for estimation of the characterisation of coronary plaques: validation using IB-IVUS. *Radiography* 2022;**28**:61–67.
30. Arbab-Zadeh A, DeMaria AN, Penny WF, Russo RJ, Kimura BJ, Bhargava V. Axial movement of the intravascular ultrasound probe during the cardiac cycle: implications for

three-dimensional reconstruction and measurements of coronary dimensions. *Am Heart J* 1999;**138**:865–872.
31. Weissman NJ, Palacios IF, Weyman AE. Dynamic expansion of the coronary arteries: implications for intravascular ultrasound measurements. *Am Heart J* 1995;**130**:46–51.
32. Ge J, Erbel R, Gerber T, Gorge G, Koch L, Haude M, Meyer J. Intravascular ultrasound imaging of angiographically normal coronary arteries: a prospective study in vivo. *Br Heart J* 1994;**71**:572–578.
33. Erdogan E, Huang X, Cooper J, Jain A, Ramasamy A, Bajaj R, Torii R, Moon J, Deaner A, Costa C, Garcia-Garcia HM, Tufaro V, Serruys PW, Pugliese F, Mathur A, Dijkstra J, Baumbach A, Zhang Q, Bourantas CV. End-diastolic segmentation of intravascular ultrasound images enables more reproducible volumetric analysis of atheroma burden. *Catheter Cardiovasc Interv* 2022;**99**:706–713.
34. Tufaro V, Serruys PW, Raber L, Bennett MR, Torii R, Gu SZ, Onuma Y, Mathur A, Baumbach A, Bourantas C. Intravascular imaging assessment of pharmacotherapies targeting atherosclerosis: advantages and limitations in predicting their prognostic implications. *Cardiovasc Res* 2023;**119**:121–135.
35. Nicholls SJ, Ballantyne CM, Barter PJ, Chapman MJ, Erbel RM, Libby P, Raichlen JS, Uno K, Borgman M, Wolski K, Nissen SE. Effect of two intensive statin regimens on progression of coronary disease. *N Engl J Med* 2011;**365**:2078–2087.
36. Nicholls SJ, Puri R, Anderson T, Ballantyne CM, Cho L, Kastelein JJ, Koenig W, Somaratne R, Kassahun H, Yang J, Wasserman SM, Scott R, Ungi I, Podolec J, Ophuis AO, Cornel JH, Borgman M, Brennan DM, Nissen SE. Effect of evolocumab on progression of coronary disease in statin-treated patients: the GLAGOV randomized clinical trial. *JAMA* 2016;**316**:2373–2384.
37. Budoff MJ, Bhatt DL, Kinninger A, Lakshmanan S, Muhlestein JB, Le VT, May HT, Shaikh K, Shekar C, Roy SK, Tayek J, Nelson JR. Effect of icosapent ethyl on progression of coronary atherosclerosis in patients with elevated triglycerides on statin therapy: final results of the EVAPORATE trial. *Eur Heart J* 2020;**41**:3925–3932.
38. Oemrawsingh RM, Cheng JM, Garcia-Garcia HM, van Geuns RJ, de Boer SP, Simsek C, Kardys I, Lenzen MJ, van Domburg RT, Regar E, Serruys PW, Akkerhuis KM, Boersma E. Near-infrared spectroscopy predicts cardiovascular outcome in patients with coronary artery disease. *J Am Coll Cardiol* 2014;**64**:2510–2518.